THE BALTEX BRIDGE CAMPAIGN

An Integrated Approach for a Better Understanding of Clouds

BY S. CREWELL, H. BLOEMINK, A. FEIJT, S. G. GARCÍA, D. JOLIVET, O. A. KRASNOV, A. VAN LAMMEREN, U. LÖHNERT, E. VAN MEIJGAARD, J. MEYWERK, M. QUANTE, K. PFEILSTICKER, S. SCHMIDT, T. SCHOLL, C. SIMMER, M. SCHRÖDER, T. TRAUTMANN, V. VENEMA, M. WENDISCH, AND U. WILLÉN

Sensor synergy and close cooperation between experimentalists and modelers is required to gain more insight into complex cloud structures and processes.

Clouds affect our daily life in many ways. They dominate our perception of weather and, thus, have an enormous influence on our everyday activities and our health. This fact is completely at odds with our knowledge about clouds, their representation in climate and weather forecast models, and our ability to predict clouds. It is their high variability in time and space that makes clouds both hard to monitor and to model. Clouds are the major concern in the climate modeling community, as stated by the Intergovernmental Panel on Climate Change (IPCC; information available online at www.ipcc.ch) "the most urgent scientific problems requiring attention to determine the rate and magnitude of climate change and sea level rise are the factors controlling the distribution of clouds and their radiative characteristics." A similar conclusion was obtained within the Atmospheric Model Intercomparison Project (AMIP; e.g., Gates et al. 1999).

The great challenge of climate research is to correctly account for the fact that the global state of our climate system is largely driven by various small-scale processes and their interaction with each other. Clouds are the most visible examples of this situation. On a global scale, clouds have a strong cooling effect on our climate: more solar radiation is reflected back to space than thermal surface radiation is trapped in the atmosphere. However, because radiation reacts on the instantaneous cloudy atmosphere and not on some climatological mean, the physical processes leading to the overall radiative effect strongly depend on the spatial distribution and structure of clouds.

AFFILIATIONS: CREWELL, LÖHNERT, SIMMER, AND VENEMA—Meteorological Institute, University of Bonn, Bonn, Germany; BLOEMINK, FEIJT, JOLIVET, VAN LAMMEREN, AND VAN MEIJGAARD—Royal Netherlands Meteorological Institute, De Bilt, Netherlands; GARCÍA—Meteorological Institute, University of Leipzig, Leipzig, Germany; KRASNOV—IRCTR, Delft University of Technology, Delft, Netherlands; MEYWERK AND QUANTE—GKSS Research Centre, Geesthacht, Germany; PFEILSTICKER AND SCHOLL—Institute for Environmental Physics, University of Heildelberg, Heidelberg, Germany; SCHMIDT AND WENDISCH—Institute for Tropospheric Research, Leipzig, Germany; SCHRÖDER—Institute for Space Sciences, Free University of Berlin, Berlin, Germany; TRAUTMANN—German Aerospace Center, Oberpfaffenhofen, Germany; WILLÉN—Meteorological and Hydrological Institute, Norrköping, Sweden

CORRESPONDING AUTHOR: Susanne Crewell, Meteorological Institute Munich, Theresienstr. 37, 80333 Munich, Germany
E-mail: crewell@meteo.physik.uni-muenchen.de
DOI:10.1175/BAMS-85-10-1565

In final form 1 May 2004

The effect of cloud structure on solar radiative transfer is not fully understood yet. From theoretical studies it is anticipated that an inhomogeneous cloud possesses a lower mean cloud reflectance and a larger mean transmittance than its one-dimensional (1D) counterpart with the same mean cloud liquid water and optical depth, the so-called albedo bias. On the other hand, strong cloud inhomogeneities may lead to a trapping of photons in the cloud's interior, causing an enhanced absorption probability for photons compared to a 1D cloud. To further complicate this issue all these effects have strong dependencies on the solar zenith angle. For small solar zenith angles the real cloud absorption can be reduced due to photon-tunneling effects within the cloud gaps, which decrease the probability of absorption of photons on their way through the inhomogeneous clouds. For large solar zenith angles photons are likely to intercept a cloud head on, leading to immediate deep penetration of the photon and enhanced possibility for absorption within the cloud (Varnai and Davies 1999). Three-dimensional (3D) radiative transfer models are necessary to analyze these effects, but they need suitable measurements to realistically prescribe the spatial and temporal cloud variability.

Clouds are condensed water which is mainly generated by the dynamics of the atmosphere. Cloud water provides the immediate connection between radiation and dynamics both in the real world and in forecast models. Passive microwave remote sensing is by far the most direct, accurate, and cost-efficient technique to estimate cloud water content. From satellites this technique can only be used with success over large water bodies. Over land areas, the focus of BBC, only ground-based techniques are applicable, and one has to rely on indirect information from the reflection of solar radiation for estimating liquid water from satellites.

The BALTEX BRIDGE campaign (BBC) was coordinated with one enhanced observational period (EOP) of the large scale field experiment BRIDGE of BALTEX (Raschke et al. 2001). As one of the projects within the Global Energy and Water Cycle Experiment (GEWEX), BALTEX aims at an improved understanding of the hydrological cycle of a large catchment area. Clouds were the focus of two coordinated projects [the BALTEX Cloud Liquid Water Network (CLIWA-NET) and the 4D-CLOUDS project] that joined forces for BBC, together with several other partners.

CLIWA-NET. CLIWA-NET (online at www.knmi.nl/samenw/cliwa-net) was the major European activity within BRIDGE concerning cloud observations and modeling studies. Within CLIWA-NET (Crewell et al. 2002) a prototype European cloud-observing system was established during three campaigns by coordinating the use of existing ground-based passive microwave radiometers and active profiling instruments. In parallel, satellite observations of clouds from the Advanced Very High Resolution Radiometer (AVHRR) series and the Advanced Microwave Sounding Unit (AMSU) were analyzed. The first two CLIWA-NET Network campaigns (CNN I and II)

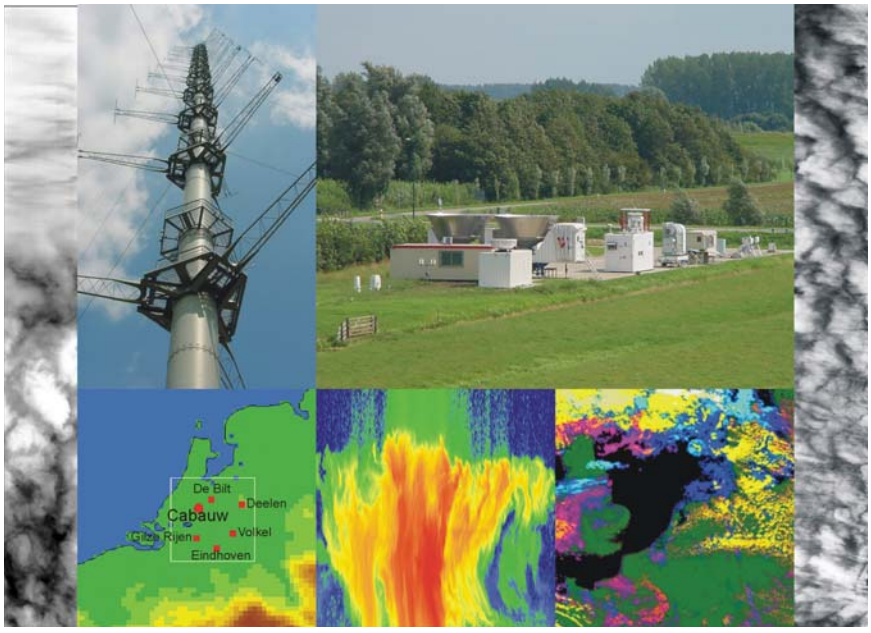

Fig. 1. Schematic overview of the BBC components: Ground-based observations from the main experimental site at Cabauw, satellite observations from AVHRR, the regional network spread in an approximately 100 km × 100 km area, and the three aircraft based in Rotterdam. Cabauw is characterized by the high meteorological tower and its lush green polder landscape. The three pictures at the bottom of the figure are the orographic map of the Netherlands with the stations of the regional network, a radar measurement of a cumulus mediocris, and a cloud classification from AVHRR. The vertical bars on both sides show CASI cloud measurements to depict the airborne component of the campaign.

were conducted on the continental scale covering the Baltic catchment, while BBC focused on the regional scale. Four European numerical weather prediction (NWP)/climate models were involved in the activities, and it was the aim of CLIWA-NET to perform an objective evaluation of their short-term cloud forecasts and to improve the parameterization of cloud processes in these models. Focus was on vertically integrated cloud liquid water and the vertical structure of clouds. Furthermore, for a future operational network a low-cost microwave radiometer was designed.

4D CLOUDS. The objective of the German 4D-CLOUDS project (information available online at www.meteo.uni-bonn.de/projekte/4d-clouds/) is an improved understanding of the effects of inhomogeneous cloud structures on transport and exchange processes in the atmosphere. All exchange processes between the earth's surface and the free atmosphere at almost all vertical levels are strongly influenced by clouds, due to dynamical, thermodynamical, and radiative effects. In general, exchange processes related to clouds are four-dimensional in nature (three spatial dimensions plus time as the fourth dimension), a fact that is often neglected in observations, as well as in large-scale dynamical models and theoretical studies. At best, one-dimensional, that is, vertically resolved, cloud structures are considered. In cloud remote sensing the three-dimensional structure is either completely ignored, or it is simply reduced to cloud cover. Within dynamical models often simple tuning factors are applied to take 3D radiative effects (e.g., cloud shadowing) into account.

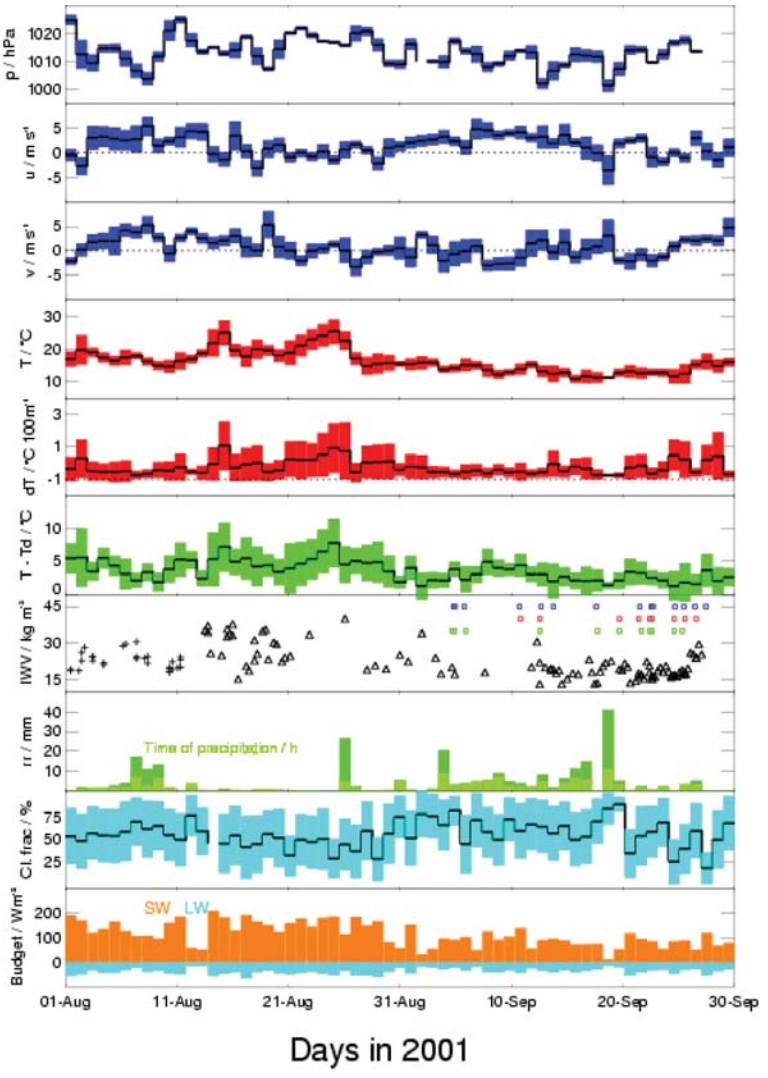

FIG. 2. Overview of meteorological conditions during BBC. Daily mean values and their standard deviation (colored range) are shown, from top to bottom, for pressure (p), west–east (u) and north–south (v) wind components, 2-m temperature (T), vertical temperature gradient (dT) from a 200-m tower and dewpoint difference ($T - T_d$), daily precipitation (rr) and daily precipitation time (dark green), cloud fraction derived from ceilometer measurements, and the shortwave (SW) and longwave (LW) radiation budget. In addition, IWV calculated from radiosondes launched during MICAM (crosses) and by the Dutch army (triangles) and the flight periods (squares) of the Partenavia (blue), Merlin (red), and Cessna (green) aircraft are shown.

BBC SETUP. The BBC was performed around a central experimental facility at Cabauw (51°58.2′N, 4°55.6′E), Netherlands. Cabauw is part of a regional network consisting of 10 remote sensing stations covering a region of 100 km × 100 km in the central Netherlands. Aircraft observations, satellite analysis, and atmospheric modeling (Fig. 1) were centered around Cabauw. The campaign lasted from 1 August until the end of September 2001. A Microwave Intercomparison Campaign (MICAM) at Cabauw marked the beginning of the campaign. After 2 weeks the microwave radiometers were distributed over the regional network that performed continuous cloud and radiation observations using lidar ceilometers, infrared radiometers, and pyranometers. In situ cloud and radiation measurements by three aircraft and a tethered balloon were performed in Septem-

ber (see Fig. 2 for time of flights). Satellite analysis and modeling efforts covered the whole campaign.

CABAUW SITE. The Cabauw Experimental Site for Atmospheric Research (CESAR; online at www.cesar-observatory.nl) about 50 km south of Amsterdam is the central measurement facility of the Royal Netherlands Meteorological Institute (KNMI), with an extensive operational measurement program. During BBC, Cabauw hosted a suite of active and passive remote sensing as well as in situ sensors (Table 1), covering a column from below the surface, throughout the boundary layer, and up to the top of the troposphere.

Radars and wind profilers. Three cloud radars operating at 3, 35, and 95 GHz, respectively, were set up next to each other within less than 30 m. Because the radar reflectivity factor is proportional to the droplet diameter to the sixth power, the radar signal backscattered by a cloud volume is dominated by large droplets. Doppler velocity and the linear depolarization (hydrometeor shape) help to distinguish between different hydrometeor types (cloud, drizzle, rain droplets, and ice particles). Most of the time, data were obtained in a vertically pointing direction (see, e.g., Fig. 3). The 95-GHz radar was, however, frequently operated in scanning mode together with a scanning microwave radiometer to investigate spatial cloud inhomogeneities. A quantitative intercomparison of the three radars revealed an accuracy of about ± 2 dB during BBC. The wind velocity and direction profile up to about 5 km and the turbulence structure in the

TABLE 1. Instrumentation operated at Cabauw, within the regional network, and on the three aircraft during BBC. The three aircraft are indicated as superscripts P [Partenavia P68B from Leibniz-Institute for Tropospheric Research (IfT)], C [Cessna C207 T from Free University (FU)], and M (Merlin IV from Météo-France]. If not annotated, the instruments belong to KNMI.

Component	Instruments	Characteristics	Derived quantities
Cabauw site	Wind profiler	Radar reflectivity profiles at 1.2 GHz; combined with RASS	Wind direction and speed
	Cloud radars	Transportable Atmospheric Radar (TARA),[d] KNMI, and Microwave Radar for Cloud Layer Exploration (MIRACLE)[e] operating at 3.35 and 95 GHz, respectively	Profiles of radar reflectivity, Doppler velocity, and linear depolarization ratio (LDR)
	Microwave radiometer	Brightness temperatures measured by five dual-frequency-channel[f,g,h,j,k] and one five-channel radiometer; two profiling systems with 12[k] and 22[b] frequency channels	Integrated water vapor (IWV), LWP, and temperature and humidity profiles
	Lidar	Backscatter profiles from single-pulse backscatter lidar[l] and four commercial lidar ceilometers (LD 40, CT75K, and CT25K)[b]	Cloud-base height
	Oxygen A-band spectrometer[m]	High spectral resolution radiances of sunlight between 760 and 780 nm	Pathlength distributions SW ↓↑, direct and diffuse
	Pyranometer	Shortwave (SW) irradiance measurements	LW ↓↑ cloud-base temperature
	Pyrgeometer	Longwave (LW) irradiance measurements	
	IR radiometer	Broadband (9.6–10.5 μm) infrared temperature by KT 19.85[b] and KT15[a,j]	
	Radiation instruments	Spectral radiometer (0.45–0.95 μm)[n], CM21, LXG500, Metek USA1, Campbell KH20,[o] digital video camera[a,o]	Spectral irradiance ↓
	Tower	Measurements at 10, 20, 40, 80, 140, and 200 m	Temperature, dewpoint, and wind direction and speed
	Sonic anemometer	Turbulence measurements using eddy correlation techniques	Sensible and latent heat flux
	Radiosondes	34 soundings using Vaisala RS-90[i] and 106 using RS-80[z] systems	Temperature, pressure, and humidity profile

lower boundary layer over Cabauw was observed by a UHF wind profiler/Radio Acoustic Sounding System (RASS; 1.29 GHz).

Lidar and ceilometers. Backscatter profiles were measured at high temporal resolution by a visible/near-infrared lidar to detect aerosol as well as ice cloud particles, and to provide data from the base of optically thick water clouds. While for this lidar a single pulse is sufficient to determine the cloud-base height, the three commercial lidar ceilometers need several seconds of integration time for this purpose. The lidar backscatter signal is proportional to the droplet diameter squared and, thus, is much more sensitive to smaller droplets compared to the radar. Therefore, radar/lidar algorithms (Donovan and van Lammeren 2001) were used to exploit the synergy by deriving profiles of ice water content and effective radius. In optically thick water clouds the lidar signal is strongly attenuated, and in most cases no information is available above approximately 200 m above cloud base.

Microwave radiometers. Microwave radiometers receive atmospheric radiation originating from water vapor, oxygen, and cloud droplets. Because the emission by clouds is proportional to the water volume, ground-based microwave remote sensing is the most accurate method to derive the vertical integral of liquid water content (LWC)—the liquid water path (LWP; Westwater 1978). For that purpose the atmospheric brightness temperature is measured at two frequencies, where one frequency has a stronger response to atmospheric water vapor while the other one is more sensitive to the cloud water. This allows the simultaneous retrieval of the integrated water va-

Table 1. Continued.

Component	Instruments	Characteristics	Derived quantities
Regional network	Microwave radiometer	Five dual-channel systems[f,g,h,j,k]	IWV, LWP
	Ceilometer	Four Vaisala CT12K and one LD40	Cloud base height
	Infrared radiometer	Broadband (9.6–10.5 μm) infrared temperature by KT19.85[b] and KT15[a,j]	Cloud-base temperature
	Pyranometer	SW irradiance measurements	SW $\downarrow$
Airborne instrumentation	Particle volume monitor	LWC of drops with diameter < 40 μm; PVM 100[c,n,p,m,b]	LWC, effective radius (r_{eff})
	Nevzorov probe[e]	Liquid and total (liquid plus ice) water content (TWC)	LWC, TWC
	FSSP	Sizing of single droplets with diameter < 40 μm; FSSP 100,[e,m] FSSP 100-ER,[e] fast FSSP[p,m]	Droplet size distribution (DSD)
	Optical array probes	Droplets with diameter between 25 and 800 μm with OAP 2D2-C[e,p,m] OAP 2D2-P[e,m]	DSD
	Aerosol sensors	Aerosol concentration for particles > 0.01 μm with 3010,[n], Passive Cavity Aerosol Spectrometer Probe (PCASP)-X[e,p]	Particle concentration and size distribution
	Albedometer[n]	1024 channels between 290 and 1000 nm; active horizontal stabilization	Spectral irradiances $\downarrow\uparrow$
	Imager	Radiances between 450 and 1000 nm by CASI[s,c]	Spectrally resolved images

[a]KNMI, De Bilt, Netherlands; [b]Meteorological Institute, University of Bonn (MIUB), Bonn, Germany; [c]Météo-France, Toulouse, France; [d]International Research Center for Telecommunications Transmission and Radar (IRCTR) Technische Universiteit Delft, Delft, Netherlands; [e]GKSS, Geesthacht, Germany; [f]Chalmers University, Gothenburg, Sweden; [g]Centre d'Etude des Environnements Terrestre et Planétaires, Velizy, France; [h]Main Geophysical Observatory, Voeykovo, Russia; [i]Met Office, Bracknell, Berkshire, United Kingdom; [j]Institute of Applied Physics, University of Bern, Bern, Switzerland; [k]DWD, Offenbach, Germany; [l]Rijksinstituut voor Volksgezondheid en Milieu, Bithoven, Netherlands; [m]Institute of Environmental Physics (IUP), Heidelberg, Germany; [n]IfT, Leipzig, Germany; [o]Technischen Universitäät (TU) Dresden, Dresden, Germany; [p]Institute for Marine and Atmospheric Research, Utrecht University, Utrecht, Netherlands; [q]Dutch army; [r]FU, Berlin, Germany

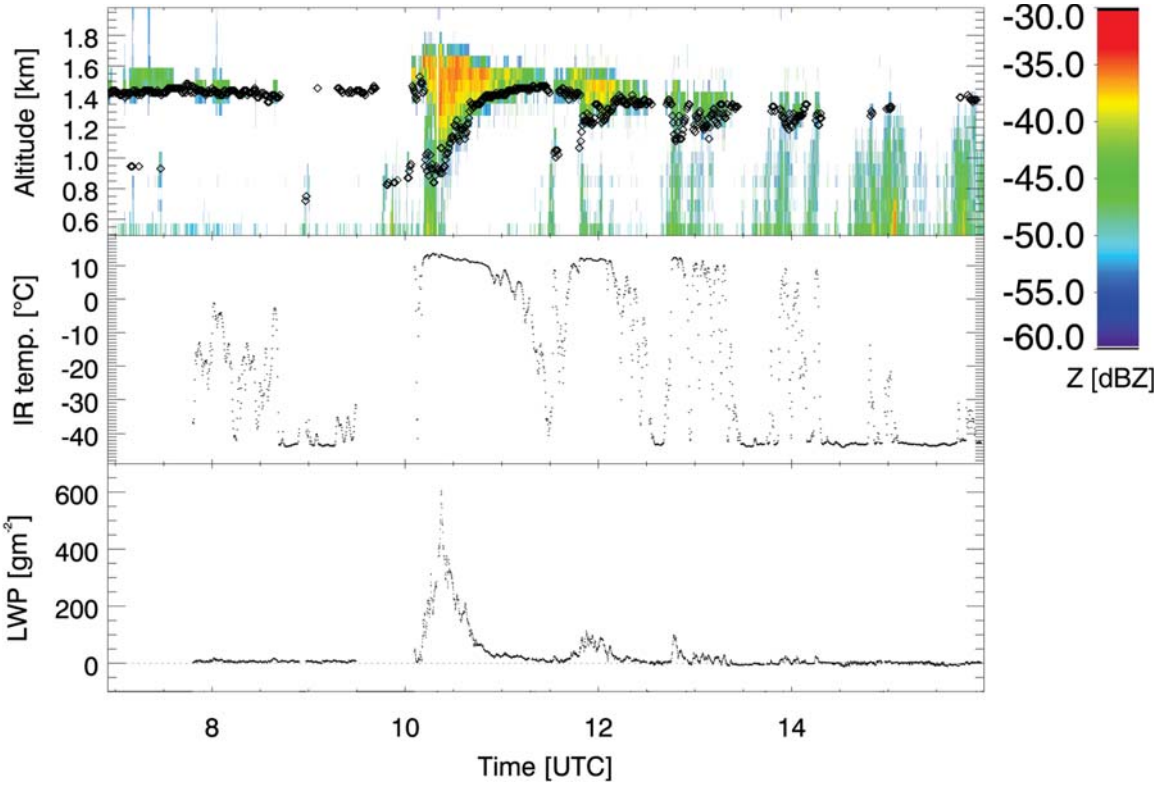

Fig. 3. Time series of radar reflectivity with overlayed cloud-base height derived from lidar ceilometer measurements (black dots), infrared temperature, and LWP measured at Cabauw on 1 Aug 2001. The radar reflections below cloud-base height are probably caused by insects, which can cause strong reflections because the radar signal is dominated by backscattering from larger targets. Hence, cloud-base information from a ceilometer is necessary to screen the radar measurements below the cloud. For clear sky the IR temperatures reflect the detection threshold around –50°C.

por (IWV). LWP accuracy depends on the frequency combination and is roughly 25 g m^{-2} (Löhnert and Crewell 2003; Crewell and Löhnert 2003). Coarse profiles of water vapor and temperature can be derived from multispectral measurements along absorption lines of water vapor and oxygen by so-called profilers. It is important to mention that precipitation reaching the instruments causes wet antennas or radomes. During these events, and some time afterward (depending on design), no useful measurements can be performed.

Eight microwave radiometers of different types participated in MICAM, including two profiler systems (Solheim et al. 1998; Crewell et al. 2001). All radiometers were placed within a radius of less than 30 m to cloud radars and lidars. In total, brightness temperatures were measured at 47 different frequencies with different bandpass characteristics, providing an unprecedented dataset for the evaluation of radiometer technology and radiative transfer model accuracy. During MICAM, 34 Vaisala RS-90 radiosondes were launched. For cloud-free conditions the data can be used directly to simulate microwave brightness temperatures. We can conclude from the MICAM comparison that the agreement between the different radiometers is in the same range as the differences between gas absorption models, like the ones of Liebe et al. (1992) and Rosenkranz (1998). The absorption of water vapor becomes more uncertain with increasing frequency.

Radiation. Multiple scattering processes determine the pathlength of individual photons on their way from the sun to the earth's surface. A high spectral resolution oxygen A-band spectrometer system was used to infer the probability density function (PDF) for pathlengths of solar photons received at the ground (see Sidebar). In the thermal infrared (IR) spectral range clouds can be regarded as blackbodies and the IR temperature measured in the presence of clouds is approximately the temperature of the cloud base (see Fig. 2). A spectral radiometer and a sun photometer were used for measuring the global and direct irradiance at the surface, respectively. Furthermore,

PHOTON PATHLENGTH DISTRIBUTION FUNCTION

The distribution of photon pathlengths may provide primary information on the atmospheric radiative transfer, which is particularly complicated for cloudy skies. Multiple scattering by cloud particles (and to a lesser extent aerosol particles) leads to randomly distributed photon paths of the transmitted or reflected solar light. In a homogeneous atmosphere where absorption with extinction ε (1/m) takes place, the atmospheric transmission as a function of wavelength can be expressed as

$$T(\varepsilon,\lambda) = [I(\lambda)/I_o(\lambda)] \,|\, [\varepsilon] = \int^P p(l) \times \exp(-\varepsilon \times 1) \times dl, \quad \text{(SB1)}$$

where $I(\lambda)$ is the light intensity received at any given point P, $I_o(\lambda)$ the incoming solar light, $p(l)$ the photon pathlength distribution function (called photon path PDF), and l is the path taken from top of the atmosphere to an observer located at P (van de Hulst 1980). In mathematical notation, the transmission $T(\varepsilon,\lambda) = I(\lambda)/I_o(\lambda)$ is a Laplace transform of the photon PDF to the argument (SB1). Thus, measurements of the transmission $T(\varepsilon,\lambda)$ as a function of ε and λ may provide primary information on the photon path PDF.

A novel method to study the cloudy sky radiative transfer, which has been developed in recent years, uses this mathematical relation. The method relies on the spectroscopic analyses of the oxygen A-band (760–780 nm) absorption in skylight being transmitted to the ground or reflected to space (Pfeilsticker et al. 1998; Min and Harrison 1999). A suite of oxygen A-band lines at high spectral resolution providing $T(\varepsilon,\lambda)$ are observed, and from Eq. (SB1) back transformation yields $p(l)$. Unfortunately, Eq. (SB1) is a mathematical ill-posed problem because the complex part of the Laplace transform cannot be measured, and, thus, the back transformation requires suitable constraints. One constraint frequently taken is to suggest the mathematical form of the photon path PDF. For example, for single- or multiple-layered but homogeneous clouds, single or multiple Γ function or lognormal distributed photon path PDFs are frequently used, whereas in broken or inhomogeneous cloud types trunctated Lévy distributions appear to be more appropriate.

measurements of the broadband solar down- and upward irradiance, longwave incoming and outgoing radiation, and multichannel infrared measurements were performed.

Turbulence and standard meteorological sensors. Profiles of wind speed and wind direction, temperature, and humidity are continuously measured at the 213-m Cabauw meteorological tower. Turbulent fluctuations of temperature and wind are estimated by a Kaijo Denki sonic anemometer at a single height (5.37 m). Infrared open-path sensors are used for humidity and carbon dioxide fluctuations. From these measurements the fluxes of momentum, sensible and latent heat, and carbon dioxide are inferred. Soil heat flux is measured with three pairs of soil heat-flux plates at –5 and –10 cm. By means of a Fourier analysis, an estimate of the surface soil heat flux is obtained. From mid-August onward the Dutch army (Landmacht) launched RS-80 radiosondes at 0300, 0900, 1500, and 2100 UTC in between the synoptic launch times (0000, 0600, 1200, and 1800 UTC) of the operational radiosonde station in De Bilt. Two tethered balloons—one equipped with standard meteorological sensors, one with microphysical measurement equipment (see below)—were operated for limited times.

AIRBORNE INSTRUMENTS. Four airborne platforms (three aircraft: Partenavia, Cessna, Merlin; and one tethered balloon), with various cloud and radiation sensors were employed (Table 1). The focus of the Partenavia flights was to measure microphysical cloud/aerosol as well as cloud radiative properties below, within, and above the clouds, while the Cessna was mainly instrumented for remote sensing above the clouds. The Merlin was additionally equipped with sensors for precipitation measurements and concentrated on measuring the microphysical properties of clouds. The tethered balloon performed high-frequency meteorological and microphysical profile soundings and turbulence measurements (Siebert et al. 2003). Beside standard meteorological and navigation instruments, the three aircraft and the balloon were equipped with numerous microphysical (droplets, aerosol particles) and radiation sensors (Table 1).

The LWC of droplets, the particle surface area density, and effective droplet radius r_{eff} (the ratio of the first two quantities) were estimated by a particle volume monitor (PVM), which makes use of the forward scattering of laser light. The Nevzorov probe is a so-called hot-wire instrument that measures the total water content (TWC) and LWC (Korolev et al. 1998). The response of the Nevzorov TWC probe

does not roll off appreciably for large droplets (Strapp et al. 2003), as it has been reported to do for the PVM (Wendisch et al. 2002). The Forward Scattering Spectrometer Probe (FSSP) and the fast FSSP [a modified version with improved electronics and slightly changed optics, see Brenguier et al. (1998)] are optical particle counters that size and count each droplet individually. The scattered light produced by a droplet when crossing a helium neon (He-Ne) laser beam is detected in the forward scattering direction, for example, between about 4° and 14°. The error of derived parameters like droplet concentration or LWC is in the range of 25%. Optical array probes (OAP) rely on shadow images of the droplets for mapping and counting (e.g., Dye and Baumgardner 1984; Gayet et al. 1993). Up- and downward solar spectral irradiances (radiative flux densities) were measured on the bottom and top of the Partenavia with a so-called albedometer, which is equipped by a unique sensor head leveling technique (Wendisch and Mayer 2003; Wendisch et al. 2001). The Compact Airborne Spectrographic Imager (CASI) mounted on the Cessna measures nadir images in the visible and near-infrared. CASI is a pushbroom imaging spectrograph, using a charge-coupled device (CCD) array as detection unit (Babey and Anger 1989; Anger et al. 1994).

SATELLITES. The AVHRR on board the National Oceanic and Atmospheric Administration (NOAA) polar orbiters has six spectral channels centered at 0.6, 0.8, 1.6, 3.7, 10.8, and 11.9 μm. The channels are optimized to measure cloud and surface characteristics with a minimum of contamination from other atmospheric constituents. During BBC, 472 overpasses of four satellites (*NOAA-12 -14, -15,* and *-16*) were processed to get spatial distributions of cloud characteristics and synoptic cloud-type classes. The KNMI's Local Implementation of Apollo Retrieval in an Operational System (KLAROS) cloud analysis shell (Feijt et al. 2002; Jolivet and Feijt 2003a,b) was used to retrieve a suite of physical cloud properties as cover fraction, cloud-top temperature, optical thickness, infrared emissivity, and LWP. KLAROS uses all spectral information for discriminating cloudy and cloud-free scenes. The quantitative cloud analysis is based on the interpretation of reflected sunlight at 0.6 μm and the emitted thermal radiation at 10.8 μm. The reflectance at 0.6 μm is converted into cloud optical depth using radiative transfer calculations. This parameter is linearly related to the LWP, assuming a constant droplet size. Information on drop size and phase (ice or water) can also be obtained from interpretation of the 1.6-μm channel available on *NOAA-15* and *-16*. During BBC, AVHRR was used to obtain spatial distributions of LWP at the time of the satellite overpass to complement the network ground-based microwave radiometers that give a high-resolution time series at one geographical location. It turns out that the improved AVHRR analysis is able to obtain LWP retrieval values that are well correlated with ground-based measurements and that are suitable for evaluation of atmospheric models.

SYNOPTIC OVERVIEW. August 2001 was a relatively warm and fairly sunny month, (Fig. 2). The period of 22–26 August marked an official heat wave and showed a strong diurnal cycle. Wind directions were mostly between the south and west-southwest (44%), with no other preferred directions. September 2001 was a cool, dull, and very wet month (Fig. 2). Spatially averaged rainfall amounted to 177 mm, compared to a long-term mean value of 71 mm. De Bilt received 211 mm, ranking this month as the second wettest September since 1901. Along the Dutch west coast, amounts were even higher with Hoek van Holland (15 km west of Rotterdam) reporting 289 mm, a record high value for September. Surprisingly, Hoek van Holland was also the sunniest spot in the Netherlands. Onshore winds prevailed with directions between the southwest and northwest (70%). These kinds of weather conditions made flight planning during BBC quite difficult.

CLOUD LIQUID WATER PATH. Continuous LWP observations were performed with the microwave radiometer for cloud carthography (MICCY) (Crewell et al. 2001) at Cabauw. Together with cloud radar, ceilometer, and infrared radiometer measurements, the cloudy sky can be described with a range of parameters. Cloud-base height from the ceilometer and temperature from the IR radiometer specify the lower cloud boundary and fix one point in the atmospheric temperature and humidity profile. High temporal fluctuations indicate broken clouds. The observed water clouds contain typically less than 100 g m^{-2}; they start precipitating when LWP reaches roughly 500 g m^{-2}. During the first day of BBC (Fig. 3) the ground-based measurements reveal a deep cloud during daytime (~1030 UTC), which crossed the measurement site in about half an hour. Later, the observed cloud passages become shorter and less deep. While the cloud vertical structure (Fig. 4) can be continuously observed from the ground, the corresponding spatial characteristics are analyzed from a satellite overpass at 1251 UTC (Fig. 5a). A cloud field consisting of convective cells with varying cell sizes

covered the Netherlands. Cells are several kilometers in diameter in the north, but in the center of the area cells may be smaller than one single AVHRR pixel (~1 km). Actually, the satellite-derived low-LWP values (10 g m^{-2}) indicate that the observed cumulus are smaller than one satellite pixel. In the vicinity of Cabauw there are also small cells with LWP values up to 80 g m^{-2}. To combine ground-based and satellite measurements the "Russian doll" method was developed.

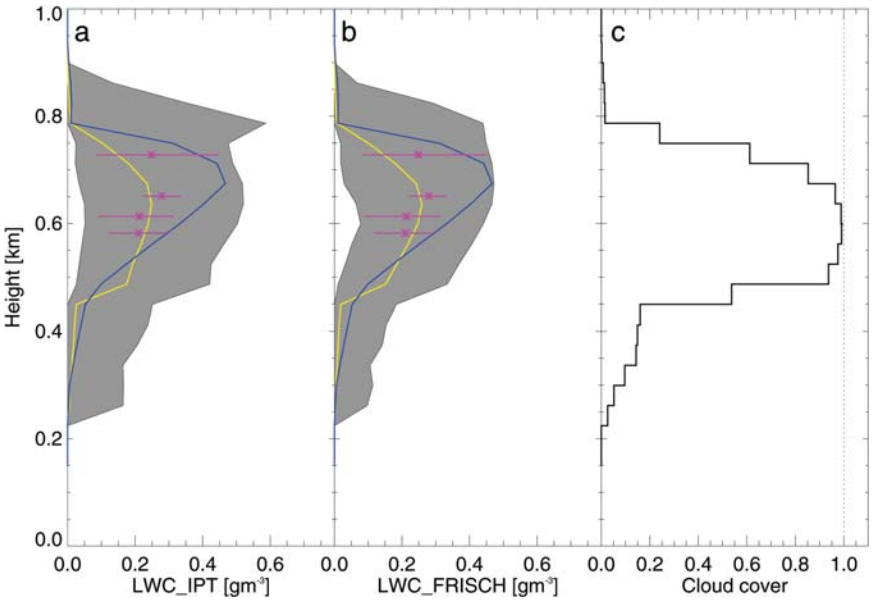

Fig. 4. Liquid water content derived from two synergetic approaches at Cabauw between 0758 and 0957 UTC 23 Sep 2001. The mean profile (yellow) and the 90th percentile are shown (a) for IPT and (b) according to Frisch et al. (1998). For a better comparison also the mean adiabatic LWC profile (blue) and the range of simultaneous aircraft measurements in the vicinity to the measurement site (< 5 km) are shown. The vertically integrated LWC of the Frisch method is equal to the one derived from microwave radiometer brightness temperature measurements at four frequencies via a statistical algorithm. The temporal average is 62 g m^{-2}; for comparison, the adiabatic value is about 100 g m^{-2}. The IPT shows a slightly higher variability and a mean LWP of 64 g m^{-2}. (c) Gaps in cloud cover lead to the smooth mean LWC profile in the upper cloud part.

THE RUSSIAN-DOLL METHOD. Clouds are highly variable in time and space. Fair weather cumulus may condense, grow, and evaporate again within less than 10 min. Therefore, it is not feasible to characterize individual clouds from NOAA polar satellite images. The characteristics of a cloud field, however, change more gradually. A useful comparison of a time series of measurements from the ground at one location to a spatial distribution obtained from a satellite at one moment in time calls for the identification of fractions of the time series and of the satellite image representative of the same cloud field. Within the Russian-doll method, the mean and the standard deviation are calculated over increasingly larger area/time intervals (in a way resembling how Russian dolls fit into each other). For 1 August, the Russian-doll graphs (Fig. 5) show the high variance at small scales, which was expected for cumulus clouds. For larger scales (about 1 h and 1 km^2), both satellite and ground-based values stabilize at a mean LWP of about 20 g m^{-2}. The method shows that a direct quantitative comparison (linking a time scale to one specific spatial scale) is not feasible in this case. Furthermore, it gives confidence that the satellite LWP values are in error not more than 20%.

CLOUD LIQUID WATER PROFILES. The unique combination of remote and in situ sensors at the Cabauw site made it possible to derive LWC profiles during BBC. Several methods exist that all make use of the vertically resolved radar reflectivity (Z) measurements. Corrections of Z for absorption by atmospheric gases and cloud water must be applied, however, for higher-frequency radar, for example, 95 GHz (Meywerk et al. 2002), before further processing. Because drizzle droplets lead to a strong radar signal, the cloud-base measurements from a lidar ceilometer can be used to distinguish between clouds and drizzle below. The application of the radar/lidar technique (Baedi et al. 2000; Krasnov and Russchenberg 2002) detects drizzle even inside the lower part of the cloud. In addition, frequent false detections of clouds due to insects can be removed by sensor synergy.

The simplest method to derive the cloud liquid water profile is the direct conversion of the radar reflectivity Z to LWC via a so-called Z–LWC relation. Because Z is proportional to the sixth moment of the drop size distribution, and LWC the third, this approach can lead to errors of more than a factor of 2 even during nonprecipitating cases. Therefore, a com-

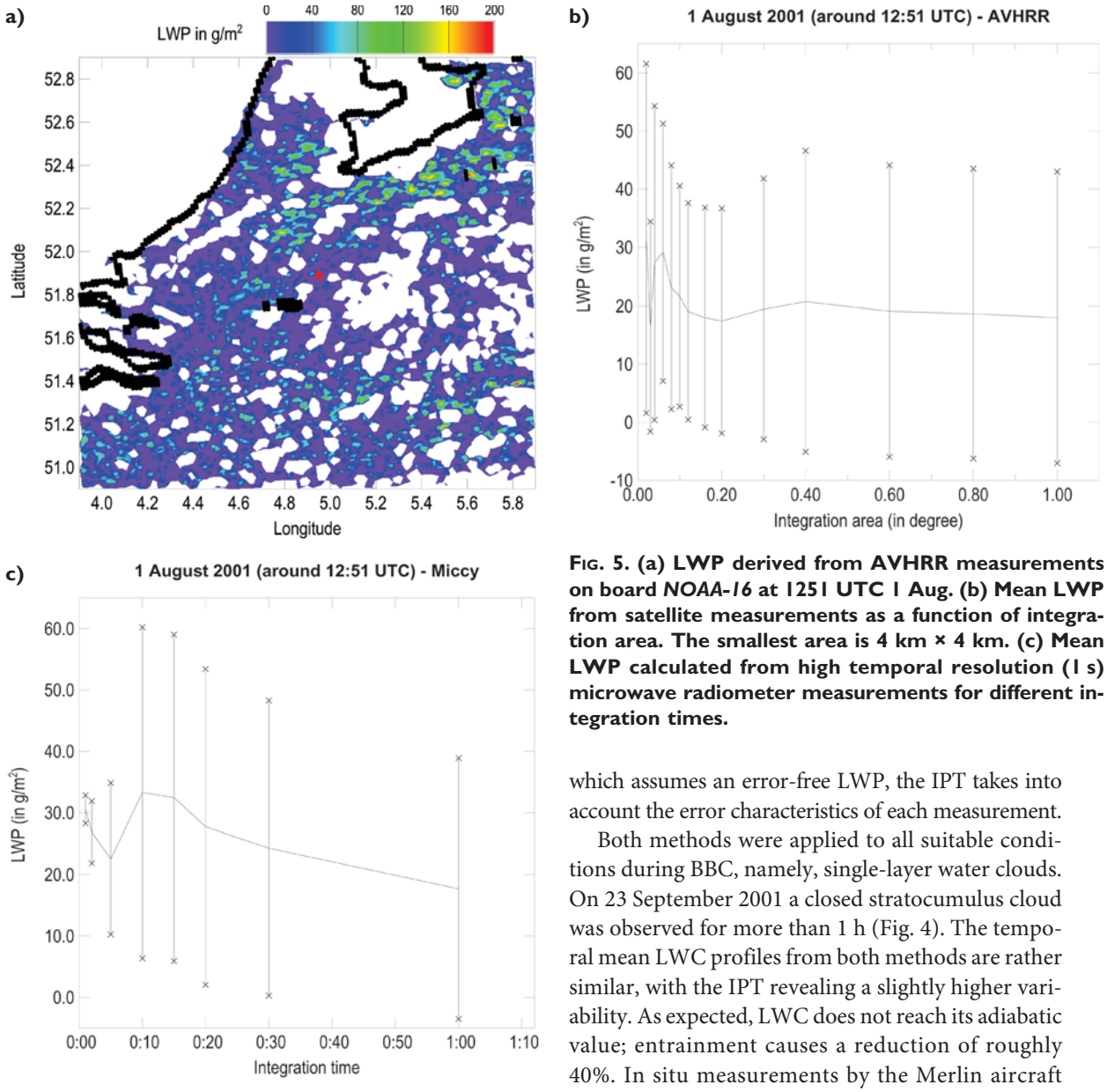

FIG. 5. (a) LWP derived from AVHRR measurements on board *NOAA-16* at 1251 UTC 1 Aug. (b) Mean LWP from satellite measurements as a function of integration area. The smallest area is 4 km × 4 km. (c) Mean LWP calculated from high temporal resolution (1 s) microwave radiometer measurements for different integration times.

mon approach according to Frisch et al. (1998) scales the radar reflectivity profile to the LWP derived from a microwave radiometer (Fig. 4). A more sophisticated technique combines the microwave brightness temperatures, the attenuation-corrected radar reflectivity profile, the lidar ceilometer cloud base, ground temperature and humidity, and the nearest operational radiosonde profile within an optimal estimation retrieval. The integrated profiling technique (IPT; Löhnert et al. 2004) developed within CLIWA-NET can simultaneously derive profiles of temperature, humidity, and LWC. The profiles retrieved with IPT are consistent with respect to the measurement error covariance, and the LWC profiles are independent of errors of an LWP algorithm. In contrast to the Frisch method, which assumes an error-free LWP, the IPT takes into account the error characteristics of each measurement.

Both methods were applied to all suitable conditions during BBC, namely, single-layer water clouds. On 23 September 2001 a closed stratocumulus cloud was observed for more than 1 h (Fig. 4). The temporal mean LWC profiles from both methods are rather similar, with the IPT revealing a slightly higher variability. As expected, LWC does not reach its adiabatic value; entrainment causes a reduction of roughly 40%. In situ measurements by the Merlin aircraft close to the Cabauw site show a similar LWC range as that derived from the ground-based sensors (Fig. 4). The high variability even in this rather homogeneous cloud field together with the very different sampling volumes of in situ and ground-based sensors limits useful validation efforts. More promising data for algorithm validation can, in principle, be provided by the tethered balloon, which can gather time series at specific cloud heights as well as profiles. Unfortunately, during BBC the weather conditions (i.e., precipitation, strong winds, multilayer clouds) did not allow for simultaneous measurements in suitable conditions.

INTERACTION OF CLOUDS AND SOLAR RADIATION. Multiple scattering and absorption of

sunlight by clouds have a significant impact on the diabatic heating in the atmosphere. The interaction of multiple scattering and absorption in cloudy atmospheres is not yet fully understood and is subject to large uncertainties, for example, in determining heating rates in global circulation models. For an improved understanding, simultaneous observations of cloud microphysical properties and corresponding radiation fields are required to validate radiative transfer calculations. Unfortunately, such four-dimensional observations are not possible; however, the combination of different approaches can reveal and quantify the relevant processes.

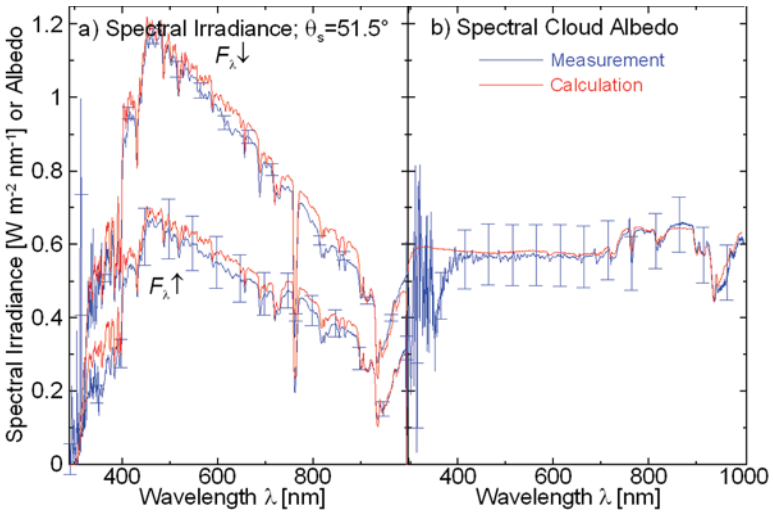

FIG. 6. Radiation measurements (blue) during a flight track less than 100 m above a cloud deck: (a) spectral downward ($F_\lambda\downarrow$) and upward ($F_\lambda\uparrow$) irradiances, and (b) derived spectral cloud albedo. The vertical bars indicate the standard deviation of the measurements along the 12-km-long (3 min) horizontal flight track. The solar zenith angle varied between θ_s = 48.7° and 48.4° during the measurement. The measurements were taken on 5 Sep 2001 (1006–1009 UTC). One-dimensional radiative transfer calculations (red) were performed on the basis of the cloud measurements shown in Fig. 7.

Spectral irradiance and microphysical measurements. The Partenavia conducted several flights in order to measure the spectral radiative properties of inhomogeneous cloud layers. As an example, observations of a specific cloud layer with a cloud top at 2.2-km altitude above ground on 5 September 2001 are analyzed. Above cloud top the sky was almost free of clouds, there were only a few cirrus (< 1/8), which barely reduced solar radiation. From the up- and downwelling spectral irradiances ($F_\lambda\uparrow$ and $F_\lambda\downarrow$, respectively) observed above the cloud deck, the spectral cloud albedo ($F_\lambda\uparrow/F_\lambda\downarrow$) is determined (Fig. 6). The absence of significant upper-level cloudiness keeps the spectrally resolved standard deviation of the downward irradiances very small. The spectral average (between 400 and 1000 nm) of the standard deviation of the downward irradiances $<\sigma\downarrow>$ is less than 0.3%. The reflected irradiances are more variable ($<\sigma\uparrow> = 4.9 \pm 1.8\%$) due to the influence of cloud-top microphysical inhomogeneities. Between 400- and 700-nm wavelengths the cloud albedo is spectrally almost constant. For larger wavelengths the high vegetation-induced surface albedo in the near-infrared causes an increase of the total albedo, most probably due to occasional cloud gaps or strong dilutions in the cloud deck. The frequent breaks in this high surface albedo regime are caused by the absorption features of oxygen and water vapor.

After this horizontal flight leg the Partenavia penetrated the cloud while descending along a slant path (Fig. 7). The cloud geometrical thickness was about 200 m, with the LWC reaching 0.2 g m^{-3} with maximum effective droplet radii of 12 μm. The downwelling irradiances (Fig. 7a) strongly fluctuate within the cloud due to cloud microphysical inhomogeneities. Also, below the cloud the downwelling irradiances vary considerably and even show some cloud-edge effects (downwelling irradiance below the cloud exceeding values above the cloud). The reflected irradiances show low variability below the cloud, but within and above the cloud the microphysical cloud inhomogeneities cause strong fluctuations in the measurements of the upwelling irradiances. To allow for comparisons with radiative transfer calculations, the spectral surface albedo was measured over several surfaces around Cabauw in cloudless conditions (Wendisch et al. 2004). However, it is quite clear that the observed fluctuations in the irradiances can not be reproduced by 1D radiative transfer calculations (Fig. 7) and the three-dimensionality of the problem needs to be addressed.

Radiative smoothing. The reflected radiance of a multilayer cloud system can substantially differ from that of a single-layer cloud due to multiple scattering between the cloud sheets. This impact is qualitatively determined by the analysis of power spectra $E(k)$ of nadir radiances observed by the Cessna aircraft. The dataset is considered to be scale invariant if $E(k) \sim k^{-\beta}$ holds, with k the wavenumber. If two ranges of scale

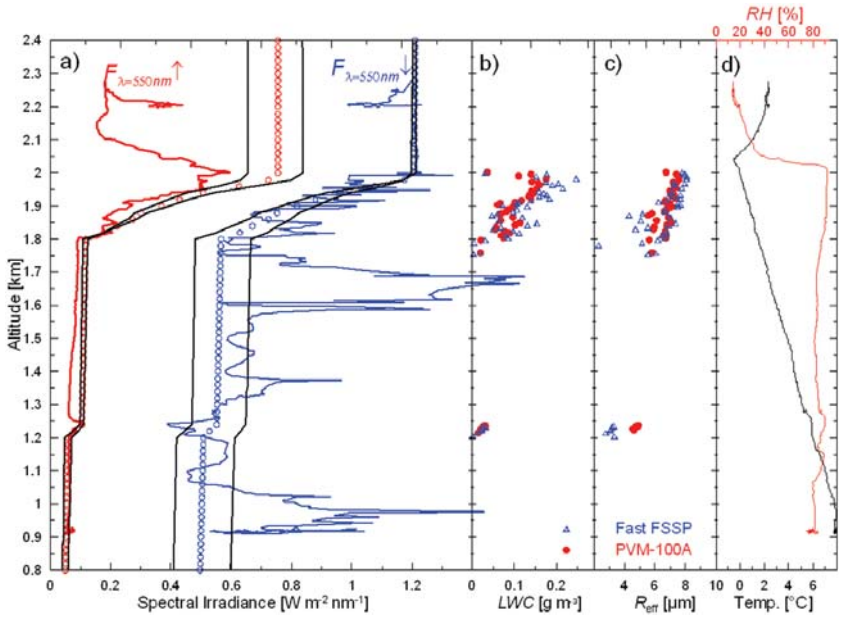

FIG. 7. Observations during a descent through a cloud immediately following the measurements shown in Fig. 6. Profiles of (a) downward (blue, $F_\lambda\downarrow$) and upward (red, $F_\lambda\uparrow$) irradiances at a wavelength of λ = 550 nm, (b) cloud LWC, (c) cloud droplet effective radius r_{eff}, and (d) air temperature (black line, lower axis) and relative humidity (red line, upper axis, RH). The blue open triangles indicate measurements with the fast FSSP, the red filled dots show PVM measurements. The measurements were taken on 5 Sep 2001 (1011–1013 UTC). The open dots in (a) mark the results of 1D radiative transfer calculations using the measured droplet size distribution (blue for downward irradiance at 550 nm, red for upward irradiances). The sensitivity of the calculations to a ± 20% change in average diameter the droplet number size is indicated by the black lines that envelop the original calculation.

invariance with a different slope β are present, the wavelength (e.g., scale), where the change in slope occurs, is called scale break (see Davis et al. 1996 for technical details).

The analysis reveals characteristic differences between data recorded above single-layer and two-layer cloud systems. The smoothing effect is evident in Fig. 1 (right-hand side), which shows the transition from a single-layer (bottom) to a two-layer cloud system (top). While the small-scale slope is almost identical in both cases, the large-scale slope of the two-layer cloud systems (1.23 ± 0.04) is 12% lower than the one for the single-cloud-layer cases (1.40 ± 0.05). This effect can be explained with an increase of radiative smoothing in the presence of a second (lower) cloud layer: optically thinner cloud parts of the upper layer appear brighter, while optically thicker cloud parts remain unchanged for nadir observations. As a consequence, less spectral energy is needed to explain the fluctuations, and the corresponding slope is lower than for a single cloud layer. The estimated scale breaks of both systems are not significantly separated and are on the order of 450 m. A more detailed discussion of the effect of two-layer clouds and surface albedo on nadir radiance observations can be found in Schröder et al. (2004).

Generally speaking, the occurrence of a scale break in power spectra of reflected solar radiation can be explained by horizontal photon transport. The nadir radiance of a specific location does not only depend on the corresponding local optical depth, but is influenced by the neighboring cloud regions due to photons traveling horizontally within the cloud (Marshak et al. 1995). The dependence of the scale break on horizontal photon transport can be interpreted as a dependence on the pathlength distribution of solar photons. We have studied conservative scattering, but it has been found recently that absorption alters the power spectral behavior significantly because long photon paths are cut off (Oreopoulos et al. 2000; Schröder and Bennartz 2003; Schröder et al. 2004).

Solar photon pathlength distributions. High spectral resolution oxygen A-band measurements aim at the detection of pathlength distributions of solar photons (PDF) transmitted through cloud covers. Derived PDFs provide integral information on atmospheric radiative transfer properties of inhomogeneous clouds (Pfeilsticker et al. 1998; Pfeilsticker 1999; Min et al. 2001) and can be used to validate 3D radiative transfer models. During BBC, technical improvements and refined retrievals allowed the photon PDFs to be computed within spatial scales smaller than the so-called radiative smoothing scale (for more details see Pfeilsticker et al. 1998 and Funk and Pfeilsticker 2003). We studied the photon PDF as a function of vertical optical depth (VOD). The photon path is usually normalized with respect to a vertical oxygen column. For a particular case on 23 September 2001 (Fig. 8) the inferred moments of the total atmospheric pathlengths are $\langle L \rangle$ = 2.84 VOD, and $\langle L^2 \rangle$ = 8.28

VOD² assuming a Γ function–shaped PDF. Hence, the mean <*L*> is significantly longer than the photon pathlength of direct sunlight (VOD = 2.2 for this solar zenith angle) would have been for a cloudless condition. Clearly the increased variance of the photon paths for cloudy skies reflects the randomization of photon paths by scattering within clouds. More details of the method (see sidebar) and their usefulness to test the hypothesis of normal versus anomalous diffusion of solar photons for cloudy skies can be found in Davis and Marshak (1997).

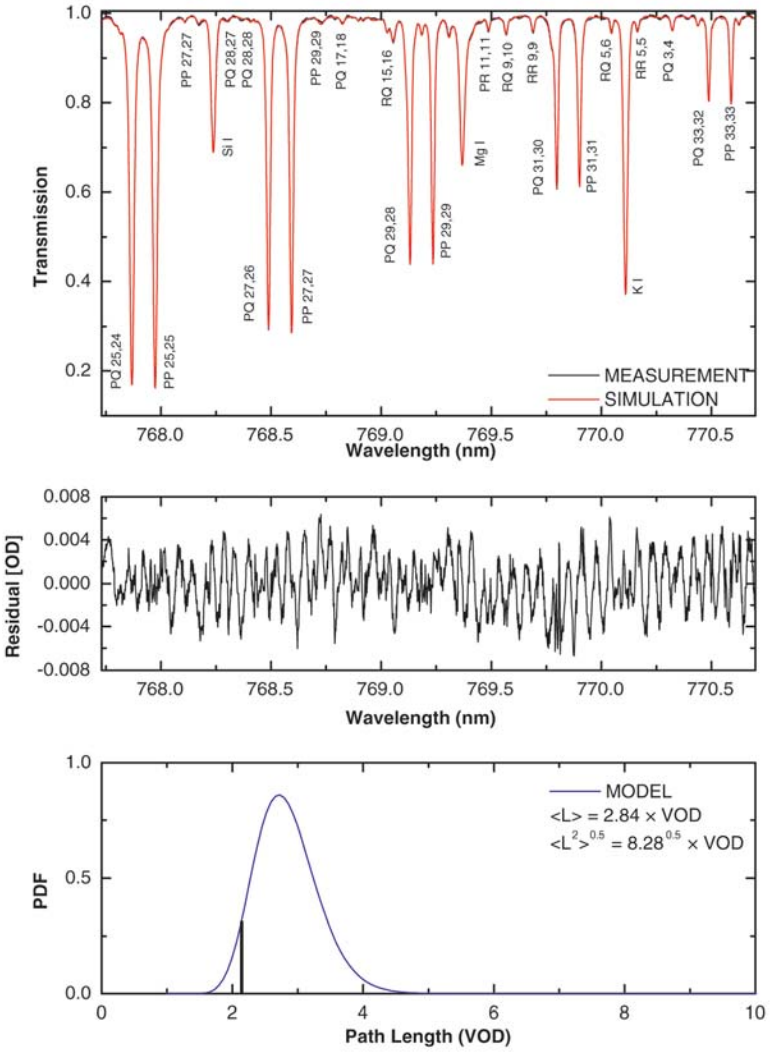

FIG. 8. Measured and modeled (top) oxygen A-band spectrum, (middle) inferred residual spectrum, and (bottom) inferred photon PDF in units of VOD for the observation between 1232 and 1233 UTC over Cabauw on 23 Sep 2001. The black vertical line in the lower panel indicates the optical path for the direct sunlight.

RADIATIVE TRANSFER MODELING. Several models are used to simulate radiative transfer in three-dimensional clouds observed during BBC. We present results obtained with the Leipzig Monte Carlo Model (LMCM), which is validated by IR3C benchmark cases, developed by the University of Leipzig based on the code by Trautmann et al. (1999). LMCM calculates the 3D field of spectral radiative flux densities in cloudy atmospheres. From these flux densities the horizontally averaged spectral reflection, transmission, and absorption, as well as the resulting solar heating rates of inhomogeneous clouds, are inferred. LMCM includes Rayleigh scattering by air molecules, extinction due to aerosol particles and cloud droplets, and absorption by various atmospheric trace gases (cf. O_3, O_2, H_2O, NO_2, etc.). Both tabulated Mie scattering phase functions as well as the Henyey–Greenstein approximation to the phase function can be employed.

With LMCM we analyzed a stratocumulus field observed during BBC on 23 September 2001. This case provides a striking example for the effect of spatial cloud variability on the reflected, transmitted, and absorbed radiative flux densities. The cloud liquid water field has been obtained as a composite from time series taken from synergetic ground-based remote sensing observations (Fig. 4). The cloud extinction field k_{ext} was calculated from LWC by assuming a constant effective radius r_{eff} = 10 μm for the cloud droplets (Slingo 1989). The time series has been converted to a 2D spatial stratocumulus cloud field by translating time into horizontal distance (x axis), based on the mean observed horizontal wind. The maximum value of k_{ext} amounts to 103.7 km^{-1}, while its average value in the entire domain is given by 7.8 km^{-1}, documenting the strong variability of the cloud. The entire cloud has a mean optical depth of about 10.

In order to assess the difference between 3D and 1D radiative transfer calculations, and to quantify the potential effect of cloud structure on the radiation field, the domain-averaged values for true and apparent (A_{true} and A_{app}, respectively) cloud absorptance were calculated as a function of wavelength (Fig. 9). Similar to standard 1D radiative transfer theory, A_{app}

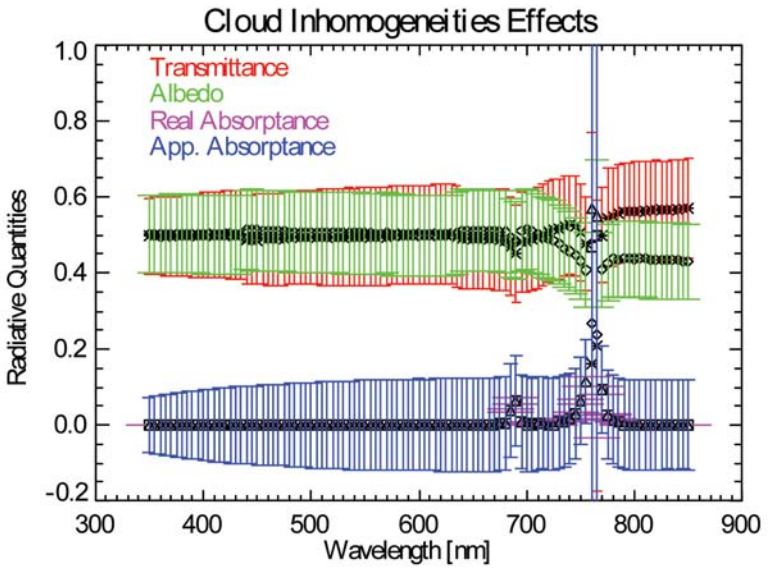

FIG. 9. Cloud transmittance (red) and cloud albedo (green), as well true (A_{true}, purple), and apparent (A_{app}, blue) cloud absorptance as a function of wavelength averaged over the full domain of the closed stratocumulus cloud deck (see Fig. 4). The bars represent the standard deviation of the respective quantities and express the influence of vertical and horizontal cloud variability on these radiation quantities. A blue bar with a length of 0.2 means that the variability of the domain-averaged apparent cloud absorptance varies between +0.1 and –0.1.

is calculated from the difference of the vertical net flux density at two levels directly below and above the cloud, thus, it does not take into account horizontal photon fluxes. Depending on cloud horizontal variability, significant over- or underestimates of the true cloud absorption for the domain average occur (see "error bars" in Fig. 9). Even for this rather homogeneous closed cloud deck, the transmission varies between 0.4 and 0.6. In this particular case A_{true} is practically zero, with the exception of the strong absorption peak in the oxygen A band near 760 nm, and the weaker absorption feature in the oxygen B band near 690 nm. Because the real mean absorptance is practically zero, the "error estimates" represent the effect of the net horizontal fluxes in the cloud, which reaches over 10%.

DYNAMIC MODEL EVALUATION. The long-term time series of continuous observations of integrated water vapor and cloud liquid water path measured during BBC allow for a statistical evaluation of NWP and climate models. In particular the cloud liquid water is of great relevance for a proper quantitative account of the cloud–radiative interactions. The daily time series of all model forecasts can be viewed online (http://cliwaftp.meteo.uni-bonn.de/CLIWANET/cliwa_dvd/

TABLE 2. Specifications of the participating atmospheric models. Here, RCM refers to regional climate model, 4DVAR to four-dimensional variational analysis, HIRLAM to the High Resolution Limited Area Model and ECHAM4 refers to the global NWP model of the Max Plank Institute of Meteorology.

	ECMWF	DWD-LM	RCA	RACMO
Institute	ECMWF	DWD	Rossby center	KNMI
Horizontal mesh (km)	~ 50	7	18	18
Vertical levels	60	35	40	24
Domain	Global	Regional	Regional	Regional
Model purpose	NWP	NWP	RCM	RCM
Assimilation	(4DVAR)	Nudging	ECMWF analysis	ECMWF analysis
Output domain	1 grid cell	7 × 7 grid cells	3 × 3 grid cells	3 × 3 grid cells
Output frequency	1 h	15 min	15 min	15 min
Remarks	Cycle 24, release 1	Nonhydrostatic dynamical core	Climate version of HIRLAM NWP	Physics from ECHAM4 GCM
Relevant references	Tiedtke (1989, 1993)	Doms and Schättler (1999)	Kain and Fritsch (1990), Rasch and Kristjansson (1998), Jones (2001)	Sundqvist et al. (1989), Roeckner et al. (1996), Christensen et al. (1996)

wp4000/select_evaltype.html). Here, we discuss the extent to which models are capable of reproducing the observed frequency distributions of IWV and LWP inferred from microwave radiometer measurements of brightness temperatures. In essence, these distributions reflect the climatology observed during the campaign.

We considered the output from model systems operational at four European institutes (Table 2). Time series output of model parameters refers to a sequence of 12–36-h time slots taken from consecutive daily forecasts initialized at 1200 UTC. Aggregation of observations to a coarser temporal resolution is carried out in order to match the model-resolved time scales. For this purpose, observations retrieved from microwave radiometer (MRAD) measurements are integrated in 10-min intervals by straightforward averaging. An important aspect in these comparisons is the fact that MRAD measurements are meaningless when the radome or antenna is wet, for example, as a result of rain. To mark such events a rain shutter mounted on the collocated IR radiometer has been used to flag the occurrence of precipitation. Once precipitation is detected in a 10-min interval, observations from this interval are rejected from further analysis. Hence, the presented values of mean observed LWP and IWV (Table 3) refer to a sample of nonprecipitative events. The duration time is given as a percentage of the total measuring time, which amounted to about 63% of the entire BBC campaign time (61 days). The model forecast series have been restricted to the time window determined from the total measuring time. This procedure ensures that the large-scale circulation statistics sampled by the model forecasts optimally resemble the observed patterns associated to the set of 10-min-observation intervals with valid cloud measurements.

Averaged over the entire sample of nonprecipitative periods two realizations occur. The models either reproduce the amount of duration time, but substantially overestimate [the European Centre for Medium-Range Forecasts (ECMWF) model, the Regional Atmospheric Climate Model (RACMO)] or underestimate [the Deutscher Wetterdienst (DWD) Lokal Modell (LM)] mean LWP, or they reproduce mean LWP, but considerably underestimate the relative occurrence [the Rossby Centre Regional Atmospheric Model (RCA)]. Mean observed IWV values are reasonably well reproduced by the models, with a tendency to slight overprediction. In the ECMWF model, cloud cover amount in the convective lower troposphere is dominated by a balance between a detrainment "source" term and a cloud erosion "sink" term (Teixeira 2001). A large eddy simulation (LES) intercomparison study by Siebesma et al. (2003) indicated that with the settings employed by the

Table 3. Relative duration *t*, mean LWP, and IWV derived from observations and model predictions. Because the "All conditions" class includes contributions from rain events, no values can be assigned to the observed mean IWV and LWP.

BBC Cabauw	All conditions			Nonprecipitating periods		
	t (%)	LWP (g m^{-2})	IWV (kg m^{-2})	*t* (%)	LWP (g m^{-2})	IWV (kg m^{-2})
Observed	100	—	—	70	38	21.6
ECMWF	100	169	23.2	67	82	22.8
LM	100	46	23.3	75	14	23.0
RCA	100	110	22.8	50	39	22.0
RACMO	100	162	23.3	74	81	22.5

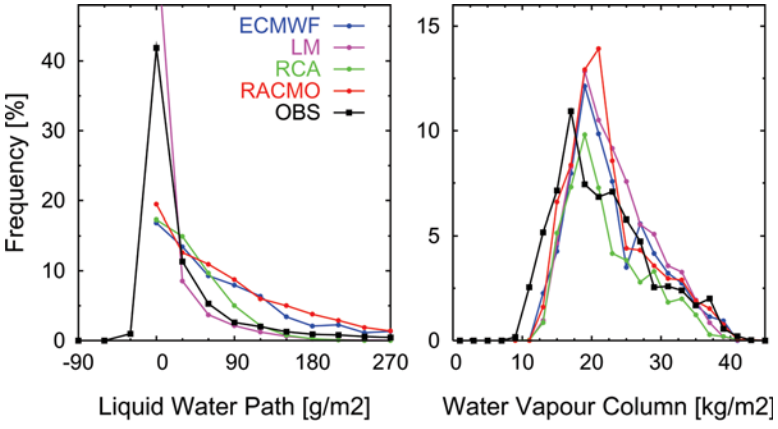

Fig. 10. Frequency distribution of observed (black) and model-predicted LWP and IWV for nonprecipitative conditions during BBC: ECMWF (blue), RCA (green), RACMO (red), and LM (magenta). Normalization is relative to the total measuring time. The corresponding mean values of LWP and IWV are listed in Table 3.

ECMWF prognostic cloud scheme (see Table 2) a quasi-steady state settles at too high values of the cloud fraction. The overprediction of LWP by the ECMWF model is probably a direct consequence of this finding. The RCA model has a tendency to convert liquid water content into precipitation at a low threshold value, which might explain its relatively low LWP and high frequency of precipitation. The found underestimation of the LM likely reflects the fact that the LWP value exported by this model carries only the resolved contribution and misses the subgrid-scale contribution associated with convection.

To examine the variance structure of observed and model-predicted LWP and IWV we compared the frequency distributions (Fig. 10) for the same conditions as discussed in Table 3. The width of the observed IWV distribution for water clouds (7.0 kg m^{-2}) is somewhat larger than the width of the model-predicted distributions, which average up to 5.9 kg m^{-2}. The excess variability in the observations might be attributed to short-term fluctuations (but longer than the 10-min-sampling interval) associated with small-scale processes that are not resolved by the models. The model-predicted frequency distributions (with the exception of the LM) show the tendency to fall off slower than the observed distribution. A possible explanation is that clouds with a vertical extension smaller than the vertical grid spacing are not resolved by the models and, hence, do not contribute to the distributions, whereas these clouds frequently occur in nature. In fact, among the models this effect is indeed stronger for RACMO with fewer model layers than ECMWF and the RCA model.

EFFECT OF VERTICAL RESOLUTION ON CLOUD STRUCTURE—A CASE STUDY. Because the vertical distribution of clouds has a large impact on the radiative heating and cooling rates of the atmosphere and the surface, we have investigated the sensitivity of the model cloud structure to the vertical resolution with BBC data. The limited horizontal and vertical resolutions of the models makes it necessary to introduce a fractional cloudiness to take into account subgrid-scale variability. Cloud radar observations were used to deduce a cloud fraction from the radar reflectivity similar to Hogan et al. (2001). The observations were temporally averaged to mimic the horizontal resolution of the RCA model.

As an example of a typical frontal passage, 18 September 2001 was picked for a sensitivity study (Fig. 11). After 1600 local time, the radar signal was dominated by rain in the lowest 3 km and the cloud-base height could not be determined. This spurious signal was removed by using the lidar ceilometer cloud-base estimates. A thin fog layer that formed in the morning hours was observed to lift around noon.

The output from the nearest grid column from RCA with three different vertical resolutions of 24, 40, and 60 vertical levels was considered. All three model runs simulate the gross cloud structure for this day with high-level clouds descending during the day and the thin low-level fog layer lifting and dissolving in the afternoon. At 60 vertical levels the model cloud fraction increases and it becomes more binary like the observations. Also, the descent of the high-level cloud and the ascent of the fog layer are somewhat better captured. Further analysis of the radar data for the whole BBC period has shown that the observed clouds are often less thick than the typical vertical grid box size (500 m–2 km) in the mid- to upper troposphere represented by 24 and 40 vertical levels. More statistical analysis is needed to assess whether the difference in the RCA cloud field with increased vertical resolution is systematic and whether it also leads to clear improvements for the radiative fluxes.

SYNTHESIS. Continuous observations are needed to better represent cloud processes in NWP and climate prediction models. Observational campaigns provide the required comprehensive datasets of dynamical, thermodynamical, and radiation parameters needed to achieve progress in the formulation of cloud parameterizations. The BBC was a step in combining observations and modeling to achieve this goal of improved parameterizations.

By integrating different ground-based remote sensing observations via an innovative algorithm, the temporal development of an atmospheric column (temperature, humidity, cloud liquid water) can be accurately described. The horizontal distribution of clouds, however, mostly in terms of vertically integrated quantities (liquid water path), can be inferred from satellite observations, but needs to be carefully matched in time and space to take into account the highly variable cloud structures. The latter becomes extremely important when the interaction of clouds with solar radiation are concerned. Clearly the assumption of horizontal homogeneity and the application of 1D radiative transfer simulations are inappropriate when microphysical cloud observations and radiation measurements should be matched. A new way to describe the 3D structure of a cloud field, and, thus, to also test our knowledge of 3D radiative transfer, might arise from high-resolution oxygen A-band spectroscopy. NWP and climate models need to parameterize the subgrid-scale effects of clouds. Within

a comprehensive evaluation of four dynamic models it became obvious that each of the models seem to have its specific model climate in terms of liquid water, and large discrepancies even between the models exist. A clear improvement could be achieved when vertical model resolution was improved to 40 or more layers to take into account the fact that many clouds are thinner than common vertical grids.

For further processing the available observations into a coherent physical representation of the local atmospheric conditions, cloud system resolving models may serve as indispensable mediators between the observations and the cloud parameterization in a large-scale model (Randall et al. 2003). In parallel, high-quality and sufficiently comprehensive observations continue to be required for the purpose of model evaluation. Such observations should be collected from independent sources, preferably long-term campaigns or routine measurements in different geographic regions, to allow for a statistical evaluation of the large-scale model under a variety of weather and climate regimes. Being sufficiently comprehensive implies that enough information can be inferred from the measurements to allow for the formulation of model-predicted quantities that are equivalent to the observed parameters. In order to serve these purposes future observational campaigns must be organized in such a way that they can meet the modeling demands. The need to measure more degrees of freedom of the cloudy atmospheric state at a higher accuracy will undoubtedly grow, because current models will continue to develop into higher complexity systems operated at higher resolutions. BBC was a first step toward achieving this goal, hopefully to be followed by similar experiments.

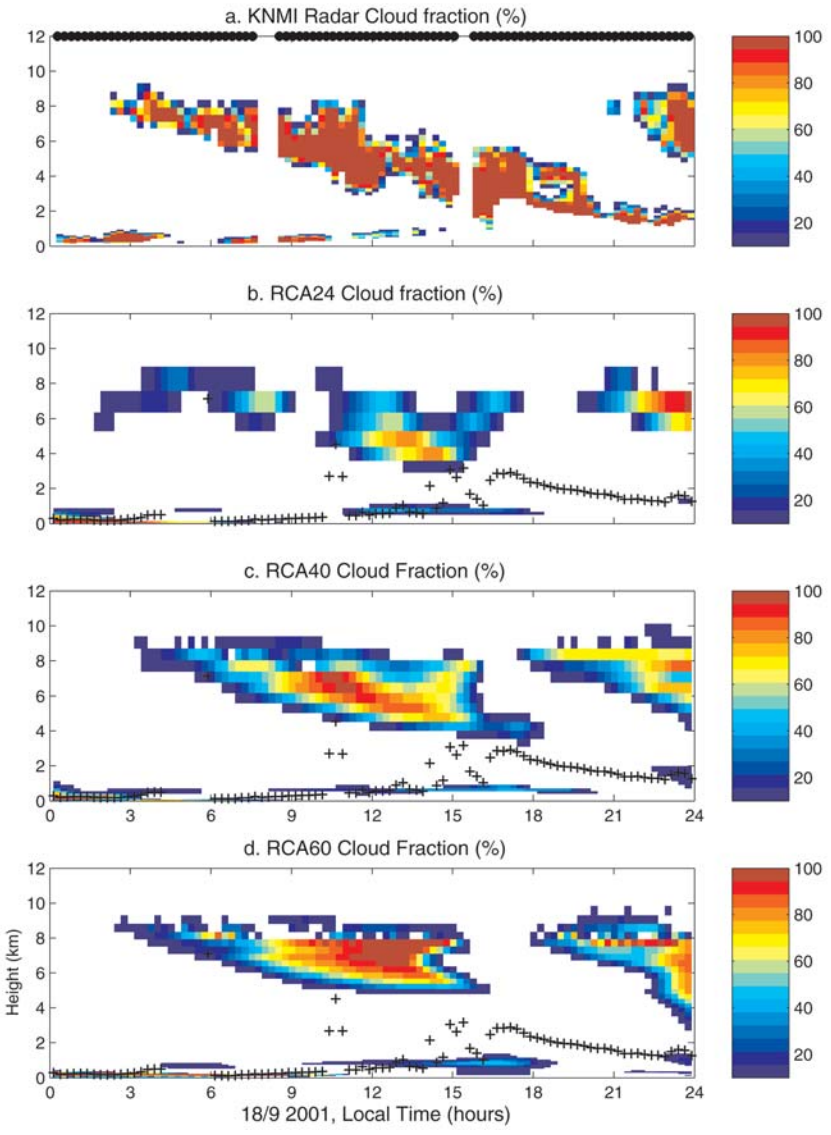

Fig. 11. Cloud fraction for 18 Sep 2001 at Cabauw (a) of the KNMI 35-GHz radar-derived cloud fraction. The black stars at the top of (a) indicate when the radar was operated. (b), (c), (d) The model cloud fractions from RCA with three different vertical resolutions are shown together with the lowest cloud base from the CTK75 lidar ceilometer indicated by black "+" signs.

Future work will concentrate on 3D radiative transfer simulations of other cloud cases observed during BBC by radar and microwave remote sensing, including airborne in situ measurements of cloud microphysics and spectral irradiances. The simulated irradiances will be compared with corresponding ground-based and aircraft measurements of the up- and downwelling spectral radiative flux densities. Statistical cloud generators and LES cloud simulations will be used to explore the impact of spatial cloud inhomogeneity on the statistics of the reflected and transmitted radiation. Finally, these investigations will

be exploited to derive a more realistic parameterization to deal with the influence of cloud inhomogeneities on the radiation fields. We invite everybody to use this wealth of observations for these and other research efforts.

ACKNOWLEDGMENTS. The BBC was made possible by contributions from the European Union (EVK2CT-1999-00007), the German Research Ministry (BMBF) as part of the 4D-CLOUDS project, the Coordinated Access to Aircraft for Transnational Environmental Research (CAATER) project, and many more international organizations. We would like to thank Colin Jones (SMHI), Felix Ament (MIUB), and Adrian Tompkins (ECMWF) for making the model output available. The success of the campaign was only possible due to the help of Jürgen Güldner, Gunnar Elgered, Lorenz Martin, Christian Mätzler, Laurent Chardenal, Cathrine Gaffard, Dagmar Nagel, Herman Russchenberg, Henk Klein Baltink, Fred Bosveld, Andreas Macke, and many more participants. Special thanks go to Wim Hovius for the excellent technical coordination of all of the measurements.

REFERENCES

Anger, C. D., S. Mah, and S. K. Babey, 1994: Technological enhancements to the Compact Airborne Spectrographic Imager (*casi*). *Proc. First Int. Airborne Remote Sensing Conf. and Exhibition,* Strasbourg, France, Environmental Research Institute of Michigan (ERIM), 205–214.

Babey, S. K., and C. D. Anger, 1989: A Compact Airborne Spectrographic Imager (*casi*). *Proc. IGARSS,* Vancouver, BC, Canada, IEEE, 1028–1031.

Baedi, R. J. P., J. J. M. de Wit, H. W. J. Russchenberg, J. S. Erkelens, and J. P. V. P. Baptista, 2000: Estimating effective radius and liquid water content from radar and lidar based on the CLARE98 data-set. *Phys. Chem. Earth B Hydrol. Oceans Atmos.,* **25,** 1057–1062.

Brenguier, J. L., T. Bourrianne, A. A. Coelho, J. Isbert, R. Peytavi, D. Trevarin, and P. Wechsler, 1998: Improvements of droplet size distribution measurements with the Fast-FSSP (Forward Scattering Spectrometer Probe). *J. Atmos. Oceanic Technol.,* **15,** 1077–1090.

Christensen, J. H., O. B. Christensen, P. Lopez, E. van Meijgaard, and M. Botzet, 1996: The HIRHAM4 Regional Atmospheric Climate Model. DMI Scientific Rep. 96-4, 51 pp. [Available from DMI, Lyngbyvej 100, DK-2100 Copenhagen, Denmark.]

Crewell, S., and U. Löhnert, 2003: Accuracy of cloud liquid water path from ground-based microwave radiometry. 2. Sensor accuracy and synergy. *Radio Sci.,* **38,** 8042, doi:10.1029/2002RS002634.

——, H. Czekala, U. Löhnert, C. Simmer, T. Rose, R. Zimmermann, and R. Zimmermann, 2001: Microwave Radiometer for Cloud Carthography: A 22 channel ground-based microwave radiometer for atmospheric research. *Radio Sci.,* **36,** 621–638.

——, M. Drusch, E. van Meijgaard, and A. van Lammeren, 2002: Cloud observations and modeling within the European BALTEX Cloud Liquid Water Network. *Bor. Environ. Res.,* **7,** 235–245.

Davis, A., and A. Marshak, 1997: Lévy kinetics in slab geometry: Scaling of transmission probability. *Fractal Frontiers,* M. M. Novak and T. G. Dewey, Eds., World Science, 63–72.

——, ——, W. J. Wiscombe, and R. Cahalan, 1996: Scale invariance of liquid water distributions in marine stratocumulus. Part I: Spectral properties and stationarity issues. *J. Atmos. Sci.,* **53,** 1538–1558.

Doms, G., and U. Schättler, 1999: *The Nonhydrostatic Limited-Area Model LM (Lokal-Modell) of DWD—Part I: Scientific Documentation,* DWD, 155 pp. [Available from Deutscher Wetterdienst, Postfach 100645, D-63004 Offenbach, Germany.]

Donovan, D. P., and A. C. A. P. van Lammeren, 2001: Cloud effective particle size and water content profile retrievals using combined lidar and radar observations. 1. Theory and examples. *J. Geophys. Res.,* **106,** 27 425–27 488.

Dye, J. E., and D. Baumgardner, 1984: Evaluation of the Forward Scattering Spectrometer Probe. Part I: Electronic and optical studies. *J. Atmos. Oceanic Technol.,* **1,** 329–344.

Feijt, A. J., D. Jolivet, and E. van Meijgaard, 2002: Retrieval of the spatial distribution of liquid water path from combined ground-based and satellite observations for atmospheric model evaluation. *Bor. Environ. Res.,* **7,** 265–271.

Frisch, A. S., C. W. Fairall, G. Feingold, T. Utal, and J. B. Snider, 1998: On cloud radar microwave radiometer measurements of stratus cloud liquid water profiles. *J. Geophys. Res.,* **103,** 23 195–23 197.

Funk, O., and K. Pfeilsticker, 2003: Photon path length distributions for cloudy skies—Oxygen A-band measurements and model calculations. *Ann. Geophys.,* **20,** 1–12.

Gates, W. L., and Coauthors, 1999: An overview of the results of the Atmospheric Model Intercomparison Project (AMIP I). *Bull. Amer. Meteor. Soc.,* **80,** 29–56.

Gayet, J.-F., P. R. A. Brown, and F. Albers, 1993: A comparison of in-cloud measurements obtained with six PMS 2D-C probes. *J. Atmos. Oceanic Technol.,* **10,** 180–194.

Hogan, R. J., C. Jakob, and A. J. Illingworth, 2001: Comparison of ECMWF winter-season cloud fraction with radar derived values. *J. Appl. Meteor.,* **40,** 513–525.

Jolivet, D., and A. Feijt, 2003a: Cloud thermodynamic phase and particle size estimation using the 0.67 and 1.6 μm channel from meteorological satellites. *Atmos. Chem. Phys. Discuss.,* **3,** 4461–4488.

——, and ——, 2003b: Retrieval of LWP fields over land from NOAA-16/AVHRR: Quantification of accuracy with objective measurements. *J. Geophys. Res.,* submitted.

Jones, C. G., 2001: A brief description of RCA2 (Rossby Centre Atmosphere Model Version 2). *SWECLIM Newsletter,* Vol. 11, 9–15.

Kain, J. S., and M. Fritsch, 1990: A 1-D entraining/detraining plume model and its application in convective parameterization. *J. Atmos. Sci.,* **47,** 2784–2802.

Korolev, A. V., J. W. Strapp, G. A. Isaac, and A. N. Nevzorov, 1998: The Nevzorov airborne hot-wire *LWC-TWC* probe: Principle of operation and performance characteristics. *J. Atmos. Oceanic Technol.,* **15,** 1495–1510.

Krasnov, O. A., and H. W. J. Russchenberg, 2002: An enhanced algorithm for the retrieval of liquid water cloud properties from simultaneous radar and lidar measurements. Vol. 1 *European Conf. on Radar Meteorology (ERAD) 2002 Proc.,* Delft, Netherlands, ERAD, 173–183.

Liebe, H. J., G. A. Hufford, and M. G. Cotton, 1992: Propagation modelling of moist air and suspended water/ice particles at frequencies below 1000 GHz. *Proc. AGARD 52nd Specialists Meeting of the Electromagnetic Wave Propagation Panel,* Palma de Mallorca, Spain, AGARD, 3-1–3-10.

Löhnert, U., and S. Crewell, 2003: Accuracy of cloud liquid water path from ground-based microwave radiometry. 1. Dependency on cloud model statistics. *Radio Sci.,* **38,** 8041, doi:10.1029/2002RS002654.

——, ——, and C. Simmer, 2004: An integrated approach toward retrieving physically consistent profiles of temperature, humidity, and cloud liquid water. *J. Appl. Meteor.,* **43,** 1295–1307.

Marshak, A., A. Davis, W. Wiscombe, and R. Cahalan, 1995: Radiative smoothing in fractal clouds. *J. Geophys. Res.,* **100,** 26 247–26 261.

Meywerk, J., O. Sievers, and M. Quante, 2002: Deriving water cloud properties from vertical pointing 95 GHz Doppler radar. Vol. 1, *Proc. Second European Conf. on Radar Meteorology* (ERAD), Delft, Netherlands, ERAD, 161–166.

Min, Q. L., and L. C. Harrison, 1999: Joint statistics of photon path length and cloud optical depth. *Geophys. Res. Lett.,* **26,** 1425–1428.

——, ——, and E. E. Clothiaux, 2001: Joint statistics of photon path length and cloud optical depth: Case studies. *J. Geophys. Res.,* **106,** 7375–7385.

Oreopoulos, L., A. Marshak, R. F. Cahalan, and G. Wen, 2000: Cloud three-dimensional effects evidenced in Landsat spatial power spectra and autocorrelation functions. *J. Geophys. Res.,* **105,** 14 777–14 788.

Pfeilsticker, K., 1999: First geometrical path lengths probability density function derivation of the skylight from spectroscopically highly resolving oxygen A-band observations. 2. Derivation of the Lévy-index for the skylight transmitted by mid-latitude clouds. *J. Geophys. Res.,* **104,** 4101–4116.

——, F. Erle, O. Funk, H. Veitel, and U. Platt, 1998: First geometrical path lengths probability density function derivation of the skylight from spectroscopically highly resolving oxygen A-band observations. 1. Measurement technique, atmospheric observations, and model calculations. *J. Geophys. Res.,* **103,** 11 483–11 504.

Randall, D., and Coauthors, 2003: Confronting models with data—The GEWEX cloud systems study. *Bull. Amer. Meteor. Soc.,* **84,** 455–469.

Rasch, P. J., and J. E. Kristjansson, 1998: A comparison of the CCM3 model climate using diagnosed and predicted condensate parameterisations. *J. Climate,* **11,** 1587–1614.

Raschke, E., and Coauthors, 2001: The Baltic Sea Experiment (BALTEX): A European contribution to the investigation of the energy and water cycle over a large drainage basin. *Bull. Amer. Meteor. Soc.,* **82,** 2389–2414.

Roeckner, E., and Coauthors, 1996: The atmospheric general circulation model ECHAM-4: Model description and simulation of present-day climate. Max Planck Institute for Meteorology Rep. 218, 90 pp. [Available from Max Planck Institute for Meteorology, Bundesstrasse 55, D-20146 Hamburg, Germany.]

Rosenkranz, P. W., 1998: Water vapor microwave continuum absorption: A comparison of measurements and models. *Radio Sci.,* **33,** 919–928. [correction in 1999, **34,** 1025.]

Schröder, M., and R. Bennartz, 2003: Impact of gas absorption and surface albedo on cloud radiative smoothing. *Geophys. Res. Lett.,* **30,** 1168, doi:10.1029/2002GL016523.

——, J. Fischer, and T. Ruhtz, 2004: Airborne remote sensing of cloud radiative smoothing during the Baltex Bridge Cloud campaign. *Atmos. Res.,* doi:10.1016/j.atmosres.2004.03.22.

Siebert, H., M. Wendisch, T. Conrath, U. Teichmann, and J. Heintzenberg, 2003: A new tethered balloon-borne turbulence platform for fine-scale observations

within the cloudy boundary layer. *Bound.-Layer Meteor.,* **106,** 461–482.

Siebesma, A. P., and Coauthors, 2003: A large eddy simulation intercomparison study of shallow cumulus convection. *J. Atmos. Sci.,* **60,** 1201–1219.

Slingo, A., 1989: A GCM parameterization for the shortwave radiative properties of water clouds. *J. Atmos. Sci.,* **46,** 1419–1427.

Solheim, F., J. Godwin, E. R. Westwater, Y. Han, S. Keihm, K. Marsh, and R. Ware, 1998: Radiometric profiling of temperature, water vapor and cloud liquid water using various inversion methods. *Radio Sci.,* **33,** 393–404.

Strapp, J. W., and Coauthors, 2003: Wind tunnel measurements of the response of hot-wire liquid water content instruments to large droplets. *J. Atmos. Oceanic Technol.,* **20,** 791–806.

Sundqvist, H., E. Berge, and J. E. Kristjansson, 1989: Condensation and cloud parameterization studies with a mesoscale numerical weather prediction model. *Mon. Wea. Rev.,* **117,** 1641–1657.

Teixeira, J., 2001: Cloud fraction and relative humidity in a prognostic cloud scheme. *Mon. Wea. Rev.,* **129,** 1750–1753.

Tiedtke, M., 1989: A comprehensive mass flux scheme for cumulus parameterization in large-scale models. *Mon. Wea. Rev.,* **117,** 1779–1800.

——, 1993: Representation of clouds in large-scale models. *Mon. Wea. Rev.,* **121,** 3040–3061.

Trautmann, T., I. Podgorny, J. Landgraf, and P. J. Crutzen, 1999: Actinic fluxes and photodissociation coefficients in cloud fields embedded in realistic atmospheres. *J. Geophys. Res.,* **104,** 30 173–30 192.

van de Hulst, H. C., 1980: *Multiple Light Scattering by Small Particles.* Dover Publications, 470 pp.

Varnai, T., and R. Davies, 1999: Effects of cloud hetereogeneities on shortwave radiation: Comparison of cloud-top variability and internal heterogeneity. *J. Atmos. Sci.,* **56,** 4206–4224.

Wendisch, M., and B. Mayer, 2003: Vertical distribution of spectral solar irradiance in the cloudless sky: A case study. *Geophys. Res. Lett.,* **30,** 1183, doi:10.1029/2002GL016529.

——, D. Müller, D. Schell, and J. Heintzenberg, 2001: An airborne spectral albedometer with active horizontal stabilization. *J. Atmos. Oceanic Technol.,* **18,** 1856–1866.

——, T. J. Garrett, and J. W. Strapp, 2002: Wind tunnel tests of the airborne PVM-100A response to large droplets. *J. Atmos. Oceanic Technol.,* **19,** 1577–1584.

——, and Coauthors, 2004: Airborne measurements of areal spectral suface albedo over different sea and land surfaces. *J. Geophys. Res.,* **109** (D08203), doi:10.1029/2003JD004392.

Westwater, E., 1978: The accuracy of water vapor and cloud liquid determination by dual-frequency ground-based microwave radiometry. *Radio Sci.,* **13,** 667–685.